

---

# MULTI-SOURCE DEEP GAUSSIAN PROCESS KERNEL LEARNING

---

A PREPRINT

**Chi-Ken Lu**

Mathematics and Computer Science  
Rutgers University Newark, NJ 07102

**Patrick Shafto**

Mathematics and Computer Science  
Rutgers University Newark, NJ 07102

February 10, 2020

## ABSTRACT

For many problems, relevant data are plentiful but explicit knowledge is not. Predictions about target variables may be informed by data sources that are noisy but plentiful, or data which the target variable is merely some function of. Intrepretable and flexible machine learning methods capable of fusing data across sources are lacking. We generalize the Deep Gaussian Processes so that GPs in intermediate layers can represent the posterior distribution summarizing the data from a related source. We model the prior-posterior stacking DGP with a single GP. The exact second moment of DGP is calculated analytically, and is taken as the kernel function for GP. The result is a kernel that captures effective correlation through function composition, reflects the structure of the observations from other data sources, and can be used to inform prediction based on limited direct observations. Therefore, the approximation of prior-posterior DGP can be considered a novel kernel composition which blends the kernels in different layers and have explicit dependence on the data. We consider two synthetic multi-source prediction problems: a) predicting a target variable that is merely a function of the source data and b) predicting noise-free data using a kernel trained on noisy data. Our method produces better prediction and tighter uncertainty on the synthetic data when comparing with standard GP and other DGP method, suggesting that our data-informed approximate DGPs are a powerful tool for integrating data across sources.

## 1 Introduction

Gaussian Process (GP) (Rasmussen and Williams, 2006) is a flexible model that imposes a prior distribution over continuous functions in Bayesian framework. For regression tasks, the ability to estimate uncertainty is the main advantage of GP over the deterministic models such as deep neural networks. This advantage originates in the assumption that the finite set of latent random variables relating to both observed and unobserved data are collectively subject to the multivariate Gaussian distribution. As such, one can elegantly formulate prediction and calibrate uncertainty within the Bayesian framework.

Two main weakness of GP are the need to choose a kernel and the lack of explicit dependence on the observations in the predictive covariance. The kernel function  $k(\mathbf{x}, \mathbf{x}')$  encodes the similarity between data  $(\mathbf{x}, y)$  and  $(\mathbf{x}', y')$ , and hence the prior distribution over functions. Typically, this must be chosen by the modeler, presumably based on knowledge of the domain. But explicit knowledge is sometimes not available, and even when it is, it can be challenging to translate knowledge into an appropriate choice of kernel. The second weakness is the lack of explicit dependence on the observations,  $y$ 's, in the predictive covariance. In standard GP, uncertainty about a predicted value  $y_*$  is completely determined by closeness of prior observations to  $x_*$  in the input space, with no influence of the actual predicted values for those prior observations. This left unjustified in most research on GPs, presumably because there are not ready methods to incorporate such a dependence.

Research has attempted to ameliorate limitations of existing kernels through composition. For example, basic operations including addition, multiplication, and convolution allow composite kernels that are more flexible than the kernels they combine (Rasmussen and Williams, 2006; Duvenaud et al., 2013). More recently, research has investigated composition of kernels. For example, one may pass the input  $\mathbf{x}$  through some deterministic transformation,  $\mathbf{x} \mapsto h(\mathbf{x})$ , which then generates the new kernel,  $k(h(\mathbf{x}), h(\mathbf{x}'))$ , with new properties within the the standard GP framework Hinton and

Salakhutdinov (2008). More generally, one may pass the input through a probabilistic transformation, for example taking the output of one GP as input into another, which gives rise to Deep GPs. Through the connection to kernel methods and Deep neural networks (Wilson et al., 2016; Raissi and Karniadakis, 2016), Deep Gaussian Processes (DGPs) (Damianou and Lawrence, 2013) and warped GPs (Snelson et al., 2004; Lázaro-Gredilla, 2012) can be regarded as a probabilistic generalization of kernel composition. Indeed, the Deep GP prior is non-Gaussian, consistent with increased expressiveness as compared to GPs, which leads to challenges for inference. Although increased expressiveness is useful in allowing application across domains, it is not the same as incorporating knowledge about a domain, which enables strong inference from limited observations.

A less obvious benefit from DGP is that the stacking structure is suitable for fusing the collection of data coming from different sources before making prediction (Perdikaris et al., 2017; Cutajar et al., 2019). For example, one may consider the regression task in which the accurate observations  $\{\mathbf{X}_r, \mathbf{y}_r\}$  are rare but very close to the ground truth while there is large amount of less precise data  $\{\mathbf{X}_p, \mathbf{y}_p\}$  available. Ideally, the plentiful data could be used to produce more informative prior while the more precise data could help reduce the uncertainty. More generally, one may consider a regression task in which the desired observations are rare, and one has access to large amount of relevant data. Relevant data may inform or constrain inference without being sampled from the target function itself. By training on this relevant data, one could construct a domain specific kernel that leverages very general knowledge about the domain—that two variables are related—and the kernel would then encode this knowledge in a way that could inform predictions of new variables based on limited observations.

In this paper, we propose a novel DGP structure in which the hidden layer connecting the input emits the random function  $h(\mathbf{x})$  sampled from the posterior distribution summarizing the data from the source variable. The next hidden layer then emits random function  $f(h)$  sampled from standard GP, which connects with the output. To tackle the intractability of inference, we follow the method of moments. Thus, we approximate our prior-posterior DGP with GP Lu et al. (2019). We shall show that the present approach can address the two weakness of standard GP mentioned above. The effective kernel captures long-range and multi-scale correlation via marginalized composition, and it also obtains explicit dependence of the observations through posterior mean. In comparison with directly applying GP on union of noisy and noise-free data, our multi-source GP shows reduced uncertainty and greater accuracy when predicting based on limited data. Experiments on synthetic multi-fidelity data also present better accuracy and tighter uncertainty in comparison with other DGP model and direct application of RBF-GP GPy (2012) with the rare data.

## 2 Related Works

The machine learning tasks with data from multiple sources have been studied in the contexts of multi-fidelity learning (Kennedy and O’Hagan, 2000; Raissi and Karniadakis, 2016; Perdikaris et al., 2017; Cutajar et al., 2019) and multi-output learning (Álvarez and Lawrence, 2011; Moreno-Muñoz et al., 2018; Kaiser et al., 2018; Kazlauskaitė et al., 2019; Janati et al., 2019). The kernel learning appeared in the literature of deep neural networks (Neal, 2012; Williams, 1997; Cho and Saul, 2009; Poole et al., 2016; Lee et al., 2017; Daniely et al., 2016; Agrawal et al., 2020) and neural tangent kernel (Jacot et al., 2018; Karakida et al., 2019; Yang, 2019). Hinton and Salakhutdinov (2008); Wilson et al. (2016); Raissi and Karniadakis (2016) demonstrated learning of the composition in kernel function through deep models.

The approach in our paper is different from the multi-fidelity DGP (Cutajar et al., 2019) which relies on inducing points (Snelson and Ghahramani, 2006; Titsias, 2009; Titsias and Lawrence, 2010) and variational inference Salimbeni and Deisenroth (2017). In the prediction stage, Cutajar et al. (2019) relies on the Monte Carlo sampling but our method does not.

Student-t process is the only stochastic model known, to our knowledge, to possess the capacity of outputting the predictive covariance which depends on the observations Shah et al. (2014).

## 3 Gaussian Process and Deep Gaussian Process

Gaussian Process (GP) is the continuum generalization of multivariate Gaussian distribution over a set of random variables denoted by  $\mathbf{f} := \{f_i\}_{i=1:N}$ . As the joint distribution  $p(\mathbf{f}) = \mathcal{N}(\mathbf{v}, K)$  is specified by the mean vector  $\mathbf{v}$  of size  $N$  and kernel matrix  $K$  of size  $N \times N$ , the distribution over the function is labeled as  $f \sim \mathcal{GP}(\mu(\mathbf{x}), k(\mathbf{x}, \mathbf{x}'))$  where, due to the marginal property of Gaussian distribution, the mean function  $\mu(\cdot)$  and kernel function  $k(\cdot, \cdot)$  generalize their counterparts in discrete case. GP regression is related to kernel ridge regression. One can regard the set of kernel functions  $\{k(\mathbf{x}_i, \cdot)\}_{i=1:M}$  evaluated at the training input  $\{\mathbf{x}_i\}_{i=1:M}$  as a basis in standard linear regression with regularization (Steinke and Schölkopf, 2008). For the zero-mean case, the conditional distribution  $p(y_* | \mathbf{x}_*, \mathbf{X}, \mathbf{y})$  associated with the function value  $f_*$  at new input  $\mathbf{x}_*$  is still a Gaussian,  $\mathcal{N}(\mu_*, \sigma_*^2)$ , with the predictive mean and

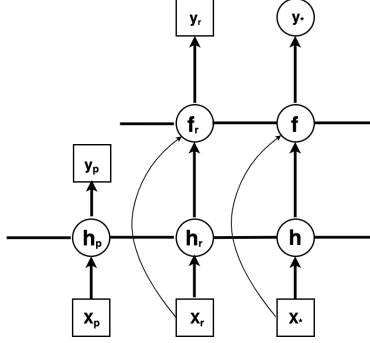


Figure 1: The diagram of the multi-source DGP model in which the two sources of data, plentiful  $\{\mathbf{X}_p, \mathbf{y}_p\}$  and rare  $\{\mathbf{X}_r, \mathbf{y}_r\}$ , are fused. The first latent layer representing the random function  $h$  has multivariate Gaussian distribution conditioned on the plentiful data and kernel function  $k_1$ . The second latent random function  $f$  has input in  $h$  and  $\mathbf{x}$  (illustrated by the curved arrow), follows the zero mean multivariate Gaussian distribution conditioned on  $h$  and kernel function  $k_2$ . The rare data is the observations connected with  $f$ . The goal is the prediction of  $y_*$  for the input at  $\mathbf{x}_*$ .

variance,

$$\mu_* = \mathbf{k}(\mathbf{x}_*, \mathbf{X})K^{-1}(\mathbf{X}, \mathbf{X})\mathbf{f} \quad (1)$$

and

$$\sigma_*^2 = k(\mathbf{x}_*, \mathbf{x}_*) - \mathbf{k}(\mathbf{x}_*, \mathbf{X})K^{-1}(\mathbf{X}, \mathbf{X})\mathbf{k}(\mathbf{X}, \mathbf{x}_*), \quad (2)$$

respectively. The above can be easily adapted to connect with noisy observations  $\mathbf{y}$ , and the hyperparameters in the kernel are determined by optimizing the marginal likelihood for the training observations.

The kernel function  $k$  is key to the properties of function  $f$  sampled from GP. Squared exponential kernel  $k(\mathbf{x}, \mathbf{x}') \propto \exp(-|\mathbf{x} - \mathbf{x}'|^2/2\ell^2)$  is a common model for smooth functions whereas the non-stationary Brownian motion kernel can generate stochastic non-differentiable continuous functions. New kernels  $k(h(\mathbf{x}), h(\mathbf{x}'))$  can be generated by a simple trick in which one composes a deterministic transformation  $h$  with a standard GP kernel. For example, passing the data through  $h(x) = x^2$  before an SE kernel allows functions of multi-length scale.

Deep Gaussian Process (DGP) Damianou and Lawrence (2013) generalizes GP the composition trick by passing the input through a GP instead of a deterministic transformation. Marginalizing the random transformation  $h$  in the latent layers, the DGP prior distribution reads,

$$p(\mathbf{f}|\mathbf{X}) = \int d\mathbf{h} p(\mathbf{f}|\mathbf{h})p(\mathbf{h}|\mathbf{X}), \quad (3)$$

where the intractable marginalization arises because the random variables  $\mathbf{h}$  appear in the inverse of kernel matrix in the GP connecting to final layer  $f$ . Deeper models can be straightforwardly obtained by inserting more latent layers  $\mathbf{h}_{1:L}$  in Equation 3.

The variational inference method Hensman et al. (2013); Salimbeni and Deisenroth (2017) tackles the intractable marginalization by introducing inducing inputs in each layer and assuming the corresponding function values are from some tractable distribution. Although the approximate inference is effective, the approximate posterior distributions over these latent functions did not capture some non-Gaussian properties such as the multi-modalness Havasi et al. (2018); Lu et al. (2019).

## 4 From DGP to Kernel Learning

Although the form of distribution in Equation 3 is not known exactly due to the intractable marginalization over latent function layers, Lu et al. (2019) studied the second and fourth moments of the DGP models where squared exponential and squared cosine covariance functions are employed in the final layer connecting to observations. Their study suggested that the two-layer DGP distribution is heavier-tailed and the joint distribution  $p(\mathbf{f}, \mathbf{h}|\mathbf{X})$  has the invariant symmetry under  $\mathbf{h} \rightarrow -\mathbf{h}$  if both conditional distributions in Equation 3 are zero-mean. Such zero-mean assumption is justified because the latent function variables, e.g.  $\mathbf{h}$ , are not connected with any observation.

In the context of multi-source data regression, GPs are very useful for modeling the general relation between mutually dependent observations from different sources (Kaiser et al., 2018; Cutajar et al., 2019). Instead of selecting some

predetermined mean function for intermediate GP in the warped GP approach (Snelson et al., 2004; Kaiser et al., 2018), we follow the DGP structure and direct part of the observations to connect with the latent function (Cutajar et al., 2019) so that the conditional distribution in Equation 3 can be posterior distribution given the partial data. More explicitly, referring to Fig. 1, we consider the collection of plentiful and rare data denoted by  $\mathcal{D}_p = \{\mathbf{X}_p, \mathbf{y}_p\}$  and  $\mathcal{D}_r = \{\mathbf{X}_r, \mathbf{y}_r\}$ , and extend the DGP model to take into account that the latent layer represents the random functions from the posterior distribution given  $\mathcal{D}_p$ ,

$$p(\mathbf{f}|\mathbf{X}, \mathcal{D}_p) = \int d\mathbf{h} p(\mathbf{f}|\mathbf{h})p(\mathbf{h}|\mathbf{X}, \mathcal{D}_p). \quad (4)$$

The DGP distribution in Equation 4 can be considered as prior over the composite functions taking into account the partial data. For convenience, we extend the notation in Lu et al. (2019) to represent the two-layer DGP. For instance,  $\text{SE}[\text{NN}|\mathcal{D}_p]$  stands for the structure associated with Equation 4 where the second layer  $f$  connecting with output is zero-mean GP with SE kernel function while the first layer  $h$  connecting with input is posterior distribution given  $\mathcal{D}_p$  and kernel function is the neural network (NN) covariance function (Williams, 1997). In the followings, we shall extract the second and fourth moments of two families of DGP models,  $\text{SE}[\cdot|\mathcal{D}_p]$  and  $\text{SC}[\cdot|\mathcal{D}_p]$  where the first layer GP can use arbitrary kernel function.

#### 4.1 Squared Exponential Composition: $\text{SE}[\cdot|\mathcal{D}]$

Here we shall evaluate the expectation values  $\mathbb{E}[f_i f_j]$  and  $\mathbb{E}[f_i f_j f_l f_m]$  associated with the DGP distribution  $p(\mathbf{f}|\mathbf{X}, \mathcal{D})$  in Equation 4. For the second moment, the marginal property of Gaussian and the integration with respect to the exposed terms  $f$ 's allow us not to confront with marginalizing out the  $h$ 's being in the inverse of covariance matrix in  $p(\mathbf{f}|\mathbf{h})$ . Instead, only the tractable integral one needs to perform is  $\int d\mathbf{h} k_2(h_i, h_j) p(\mathbf{h}|\mathbf{X}, \mathcal{D})$ . It is convenient to write the square in quadratic form,  $(h_i - h_j)^2 = [\mathbf{h}]_{ij}^T \mathbb{J}_2 [\mathbf{h}]_{ij}$  where the notation for the two-entry column vector  $[\mathbf{h}]_{ij} = \begin{pmatrix} h_i \\ h_j \end{pmatrix}$  and the two-by-two matrix  $\mathbb{J}_2 = \begin{pmatrix} 1 & -1 \\ -1 & 1 \end{pmatrix}$  have been used. Therefore, the SE covariance function in the layer connecting with output now reads,

$$k_2(h_i, h_j) = \sigma_2^2 \exp \left[ -\frac{[\mathbf{h}]_{ij}^T \mathbb{J}_2 [\mathbf{h}]_{ij}}{2\ell_2^2} \right]. \quad (5)$$

The marginal property of Gaussian again simplifies the integration into

$$\mathbb{E}[f_i f_j] = \int d[\mathbf{h}]_{ij} k_2(h_i, h_j) \mathcal{N}([\mathbf{h}]_{ij} | \mathbb{V}_2, \mathbb{K}_2), \quad (6)$$

where the two-entry posterior mean vector

$$\mathbb{V}_2 = \begin{pmatrix} \mu_i \\ \mu_j \end{pmatrix},$$

and the two-by-two covariance matrix,

$$\mathbb{K}_2 = \begin{pmatrix} k_{ii} & k_{ij} \\ k_{ij} & k_{jj} \end{pmatrix},$$

are obtained from the posterior mean and covariance matrix, respectively, given the partial data  $\mathcal{D}$ .

**Lemma 1.** *The second moment of  $\text{SE}[\cdot|\mathcal{D}]$  in Equation 6 can be shown to have the following form,*

$$\mathbb{E}[f_i f_j] = \frac{\sigma_2^2}{\sqrt{D_{ij}}} \exp \left[ -\frac{(\mu_i - \mu_j)^2}{2\ell_2^2 D_{ij}} \right] \quad (7)$$

where the symbol  $D_{ij} = 1 + (k_{ii} + k_{jj} - 2k_{ij})/\ell_2^2$  represents the determinant of the matrix  $I_2 + \mathbb{K}_2 \mathbb{J}_2$ .

*Proof.* Without loss of generality, we assume the hyperparameters  $\sigma_2 = \ell_2 = 1$  in the output layer. The analytic form for the second moment is given in (Lu et al., 2019),

$$\mathbb{E}[f_i f_j] = \frac{\exp(-\frac{1}{2} \mathbb{V}_2^t \mathbb{A}_2 \mathbb{V}_2)}{\sqrt{I_2 + \mathbb{K}_2 \mathbb{J}_2}},$$

where the matrix  $\mathbb{A}_2 = \mathbb{K}_2^{-1} [I_2 - (I_2 + \mathbb{K}_2 \mathbb{J}_2)^{-1}]$ . It can be shown that the involved 2-by-2 matrices satisfy the following identity,

$$I_2 - (I_2 + \mathbb{K}_2 \mathbb{J}_2)^{-1} = \frac{\mathbb{K}_2 \mathbb{J}_2}{D_{ij}}, \quad (8)$$

with which we can proceed to show  $\mathbb{A}_2 = \mathbb{J}_2/D_{ij}$  and the exponent in above reads  $-(\mu_i - \mu_j)^2/2D_{ij}$ .  $\square$

The second moment captures the effective covariance generated through the marginalized composition in DGP distribution. Unlike the discussions in (Lu et al., 2019) where the GPs in latent layers are zero-mean, the presence of Gaussian posterior in DGP allows the effective covariance function in Equation 7 to depend on the posterior mean given the partial data, which is a novel method of data driven composition of deep multi-scale kernels. The factor  $1/\sqrt{D_{ij}}$  reproduces the kernel for zero-mean case in which the length scales  $\ell_1$  in  $k_{ij}$  and  $\ell_2$  give rise to multi-scale correlation. Another novelty of this kernel is that the difference  $(\mu_i - \mu_j)$  between the posterior mean from first GP appears in the second factor allows the partial training observations to enter the covariance function and the ensuing predictive covariance. Standard GPs does not have the capacity of providing observation-dependent predictive covariance (Shah et al., 2014). In addition, the exponent of this factor is scaled by input-dependent length scale  $\ell_2\sqrt{D_{ij}}$ . Lastly, one can collapse the first GP into a deterministic mapping, i.e.  $\mu_i = g(\mathbf{x}_i)$ , by setting the signal magnitude  $\sigma_1 = 0$ , which leads to a transformed SE kernel function  $\mathbb{E}[f_i f_j] = \sigma_2^2 \exp[-(g_i - g_j)^2/2\ell_2^2]$ .

The statistics of DGP are not solely determined by the second and first moments, however. We can show that the fourth moment of interest can be derived in a similar manner. The calculation of higher moments for multivariate Gaussian distribution is facilitated by the theorem in (Isserlis, 1918) with which the fourth moment  $\mathbb{E}_{\mathcal{N}}[f_i f_j f_l f_m] = \sum \mathbb{E}_{\mathcal{N}}[f_a f_b] \mathbb{E}_{\mathcal{N}}[f_c f_d]$  with the summation being over all three distinct ways decomposing the quartet  $\{i, j, m, l\}$  into two doublets (for instance  $\{a, b\} = \{i, j\}$  and  $\{c, d\} = \{m, l\}$ ).

**Lemma 2.** *The fourth moment of  $SE[\cdot|\mathcal{D}]$  is given by the sum over distinct doublet decomposition and corresponding expectation values,*

$$\mathbb{E}[f_i f_j f_m f_l] = \sigma_2^4 \sum \frac{\alpha_{ab,cd} \alpha_{cd,ab} \beta_{ab,cd}}{\sqrt{D_{ab} D_{cd} - V_{ab,cd}^2}} \quad (9)$$

with  $V_{ab,cd} = (k_{ad} + k_{bc} - k_{ac} - k_{bd})/\ell_2^2$  and the expressions,

$$\alpha_{ab,cd} = \exp \left[ \frac{-(\mu_a - \mu_b)^2}{2\ell_2^2(D_{ab} - V_{ab,cd}^2/D_{cd})} \right],$$

and

$$\beta_{ab,cd} = \exp \left[ \frac{(\mu_a - \mu_b)(\mu_c - \mu_d)V_{ab,cd}}{\ell_2^2(D_{ab}D_{cd} - V_{ab,cd}^2)} \right].$$

*Proof.* We start with rewriting the product of the covariance function  $k_2(h_a, h_b)k_2(h_c, h_d) = \exp(-\frac{[\mathbf{h}]_{ab,cd}^T \mathbb{J}_4 [\mathbf{h}]_{ab,cd}}{2})$  where the row vector  $[\mathbf{h}]_{ab,cd}^T = (h_a, h_b, h_c, h_d)$  and the matrix

$$\mathbb{J}_4 = \begin{pmatrix} \mathbb{J}_2 & 0 \\ 0 & \mathbb{J}_2 \end{pmatrix}.$$

The above zeros stand for 2-by-2 zero matrices in the off-diagonal blocks. The procedure of obtaining expectation value with respect to the 4-variable multivariate Gaussian distribution  $\mathcal{N}([\mathbf{h}]_{ab,cd}|\mathbb{V}_4, \mathbb{K}_4)$  is similar to the previous one in obtaining the second moment. Namely,

$$\mathbb{E}[k_2(h_a, h_b)k_2(h_c, h_d)] = \frac{\exp(-\frac{1}{2}\mathbb{V}_4^t \mathbb{A}_4 \mathbb{V}_4)}{\sqrt{I_4 + \mathbb{K}_4 \mathbb{J}_4}},$$

in which the calculation of inverse of 4-by-4 matrix  $I_4 + \mathbb{K}_4 \mathbb{J}_4$  and its determinant is quite tedious but tractable.  $\square$

## 4.2 Squared Cosine Composition: $SC[\cdot|\mathcal{D}]$

In the present case, the second GP in Figure 1 is also zero-mean but employs the squared cosine kernel function, i.e.  $k_2(h_i, h_j) = \sigma_2^2 \cos^2 \frac{h_i - h_j}{2\ell_2}$ . After writing  $k_2(h_i, h_j) = \{2 + \exp[i(h_i - h_j)] + \exp[-i(h_i - h_j)]\}/4$ , the same trick can be applied to obtain the second moment of  $SC[\cdot|\mathcal{D}]$  DGP.

**Lemma 3.** *The second moment of  $SC[\cdot|\mathcal{D}]$  DGP distribution is*

$$\mathbb{E}[f_i f_j] = \frac{\sigma_2^2}{2} [1 + \cos(\mu_i - \mu_j) \exp(V_{ij})] \quad (10)$$

where the symbol  $V_{ij} = (2k_{ij} - k_{ii} - k_{jj})/2\ell_2^2$  represents the posterior covariance from the first-layer GP.

*Proof.* The above follows from the expectation value identity  $\int d[\mathbf{h}]_{ij} e^{\mathbf{a}^T [\mathbf{h}]_{ij}} \mathcal{N}([\mathbf{h}]_{ij} | \mathbf{u}, \Sigma) = \exp(\mathbf{a}^T \mathbf{u} + \mathbf{a}^T \Sigma \mathbf{a} / 2)$  along with the identification of vector  $\mathbf{a} = \pm(i, -i)^T$ .  $\square$

Similarly, the fourth moment of  $\text{SC}[\cdot | \mathcal{D}]$  also has closed form in the following lemma.

**Lemma 4.** *The fourth moment is a sum over all three partition of quartet into pair of doublets, and the relation with the second moment is given by,*

$$\begin{aligned} \mathbb{E}[f_i f_j f_m f_l] = \sum \mathbb{E}[f_a f_b] \mathbb{E}[f_c f_d] + \frac{e^{V_{ab} + V_{cd}}}{8} \times \\ [e^{2V_{ab, cd}} \cos(\mu_a - \mu_b + \mu_c - \mu_d) + \\ e^{-2V_{ab, cd}} \cos(\mu_a - \mu_b - \mu_c + \mu_d) - \\ 2 \cos(\mu_a - \mu_b) \cos(\mu_c - \mu_d)] \quad (11) \end{aligned}$$

The proof can be found in Appendix.

### 4.3 Non-Gaussian statistics

One can determine whether a univariate distribution is heavy-tailed or light-tailed by the sign of its excessive kurtosis, and Gaussian distribution corresponds to zero. The fourth moments along with the second moments in the zero-mean two-layer DGP studied in Lu et al. (2019) suggest that both the SE[] and SC[] compositions result in heavy-tailed statistics. Nonzero posterior mean in the present two-layer DGP enriches the statistical property. First, in both SE[] and SC[] compositions, the present DGP can be a GP *if the signal  $\sigma_1 = 0$  in the first layer*, which results in zero covariance and  $D = 1$ . Moreover, one can show that the fourth moment, for instance,  $\mathbb{E}[f_1 f_2 f_3 f_4] = \mathbb{E}[f_1 f_2] \mathbb{E}[f_3 f_4] + \mathbb{E}[f_1 f_3] \mathbb{E}[f_2 f_4] + \mathbb{E}[f_1 f_4] \mathbb{E}[f_2 f_3]$ , which is signature of multivariate Gaussian distribution.

However, the presence of mean function  $\mu$  in second and fourth moments complicates the consideration for general cases. We first consider the SC composition and the simpler fourth moment  $\mathbb{E}[f_1^2 f_2^2]$ . Since we are interested in approximating DGP with GP, the fourth moment in GP approximation shall read  $\sigma_2^4 + 2(\mathbb{E}[f_1 f_2])^2$ . The true fourth moment, compared with the GP approximation, contains additional contribution proportional to,

$$e^x \cos 2\theta + e^{-x} - 2 \cos^2 \theta \geq 2 \sin^2 \theta (1 - e^x),$$

where we denote  $x = 4k_{12} - 2k_{11} - 2k_{22} < 0$  and  $\theta = \mu_1 - \mu_2$ . Therefore, this fourth moment is underestimated if one approximates this DGP with GP. In general, one could either prove that the most general fourth moment is always underestimated given any posterior mean function, or one could prove the opposite by finding a posterior mean such that the true fourth moment is smaller than the one obtained from the approximate GP. As for the SE DGP, the situation is even more complicated as the posterior mean and covariance both appear in the exponent in Equation 7 and 9, which makes the demonstration even more challenging.

### 4.4 Pathology kernels

The previous derivations show construction of effective kernel function  $k_{\text{eff}}$  in the posterior-prior stacking DGP, SE[] (Equation 7) and SC[] (Equation 10). The kernel functions depend on the input  $\mathbf{x}$ 's implicitly through the posterior mean  $\mu_{i,j}$  and covariance  $k_{i,j}$  given data  $\mathcal{D}$ . One has the freedom to include explicit dependence of input by multiplying  $k_{\text{eff}}$  with SE kernel Duvenaud et al. (2014),

$$k_{\text{path}}(\mathbf{x}_i, \mathbf{x}_j) = \sigma_2^2 \exp\left(-\frac{|\mathbf{x}_i - \mathbf{x}_j|^2}{2\ell^2}\right) k_{\text{eff}}(\mathbf{x}_i, \mathbf{x}_j). \quad (12)$$

## 5 Multi-source GP Regression

Given a set of rare observation  $\{\mathbf{X}_r, \mathbf{y}_r\}$ , the multi-source regression task is to infer the function, which has following functional dependence,

$$y = f[h(\mathbf{x}), \mathbf{x}] + \mathcal{N}(0, \sigma_n^2), \quad (13)$$

and the hidden function  $h$  can be inferred from the plentiful data  $\{\mathbf{X}_p, \mathbf{y}_p\}$ . For instance,  $f$  could represent the amount of sun exposure while  $h$  could represent temperature at an array of locations. The hierarchy of two-level inference suits with the prior-posterior DGP shown in Figure 1. Moreover, marginalization over the hidden function  $h$  is the Bayesian spirit, instead of selecting the most probable  $h$ . As shown in previous section, our approach is to approximate

**Algorithm 1** multi-source DGP kernel learning

**Input:** two sources of data, plentiful data  $(\mathbf{X}_p, \mathbf{y}_p)$  and rare data  $(\mathbf{X}_r, \mathbf{y}_r)$ , kernel functions  $k_1$  in the latent layer for  $h$ , and the new input  $\mathbf{x}_*$ .

1. Evaluate the predictive mean  $\mathbf{u}$  and covariance matrix  $\Sigma$  at input  $\mathbf{X}_r \cup \mathbf{x}_*$  from the optimized evidence of  $\mathbf{y}_p$ .
2. Construct the kernel matrix  $K$  for input from  $\mathbf{X}_r \cup \mathbf{x}_*$  using  $k_{\text{eff}}$  in Eq. 7 or 10.  $\mu_i$  and  $k_{ij}$  are entries in  $\mathbf{u}$  and  $\Sigma$ , respectively.
3. The hyperparameters  $\sigma_2$  and  $\ell_2$  in  $k_{\text{eff}}$  are determined by the optimized evidence of  $\mathbf{y}_r$ .
4. Evaluate the predictive mean  $\mu_*$  and variance  $\sigma_*$  using Eq. 1 and 2 with  $K$  and  $\mathbf{y}_r$ .

**Output:** Predictive mean  $\mu_*$  and variance  $\sigma_*$  at input  $\mathbf{x}_*$ .

the DGP with a GP in which the employed kernel function represents the nontrivial correlation and dependence on plentiful data out of the intractable marginalization over the hidden function. In passing, we note that the non-Gaussian character not captured by this approximation is related to whether outlier samples should appear more (heavy-tailed) or less (light-tailed) frequently than the multivariate Gaussian distribution can generate. Below, we shall describe our approximate inference with the effective GP model shown in Figure 2.

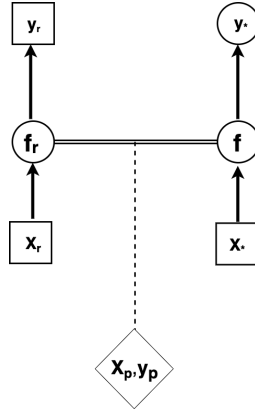


Figure 2: GP representation of multi-source DGP with kernel learned from marginalization over the posterior distribution over the latent random function  $h$  in Fig. 1 given the plentiful data  $\{\mathbf{X}_p, \mathbf{y}_p\}$ . Standard GP regression using the learned kernel demonstrates significantly reduced uncertainty with only small amount of rare data  $\{\mathbf{X}_r, \mathbf{y}_r\}$ .

The first objective is to infer the hidden function  $h$  from  $\{\mathbf{X}_p, \mathbf{y}_p\}$ . Namely, we are interested in  $\mathbf{h}_r$  and  $h_*$  evaluated at  $\mathbf{X}_r$  and  $\mathbf{x}_*$ , respectively, and they follow the joint multivariate normal distribution,

$$\begin{bmatrix} \mathbf{y}_p \\ \mathbf{h}_{r,*} \end{bmatrix} \sim \mathcal{N}\left(0, \begin{bmatrix} K(\mathbf{X}_p, \mathbf{X}_p) + \sigma_n^2 I & K(\mathbf{X}_p, \mathbf{X}_{r,*}) \\ K(\mathbf{X}_{r,*}, \mathbf{X}_p) & K(\mathbf{X}_{r,*}, \mathbf{X}_{r,*}) \end{bmatrix}\right), \quad (14)$$

given the information from the plentiful data. Consequently, the posterior distribution  $p(\mathbf{h}_r, h_* | \mathbf{X}_p, \mathbf{y}_p) = \mathcal{N}(\mathbf{u}, \Sigma)$  can be obtained by standard GP procedure. The relevant information regarding  $h$  within the posterior mean  $\mathbf{u}$  and covariance  $\Sigma$  can lead to the kernel matrix in Figure 2 at input  $\mathbf{X}_r$  and  $\mathbf{x}_*$ . Then optimization over the evidence for  $\mathbf{y}_r$  results in the corresponding hyperparameters for the effective GP. Algorithm 1 lists the summary of calculation procedure for multi-source DGP kernel learning with the rare data.

## 6 Experiments

Here, we shall demonstrate the results from our multi-source GP inference with synthetic rare and plentiful data. There are two demonstrations of data here. In the first one, the relation between the two sources of data is fixed but implicit. This type of problem is the same as that studied in multi-fidelity simulation Perdikaris et al. (2017); Cutajar et al. (2019). On the other hand, in the second type of problem the relation between noisy data and noise-free data is not through a fixed mapping. Thus, it is interesting to note that the multi-source GP inference may be analogous with the denoising autoencoder Alain and Bengio (2014); Bengio et al. (2013).

## 6.1 Two-fidelity data

We first show the example with the plentiful data generated from  $g_1(x) = x^2$  (30 data) and the rare data from  $g_2(x) = \sin 2\pi x^2$  (10 data). We apply the standard GPy regression package with RBF kernel GPy (2012) to infer the distribution over hidden function from plentiful data  $\{\mathbf{X}_p, \mathbf{y}_p\}$ . With the predictive mean  $\mathbf{u}$  and covariance matrix  $\Sigma$ , we can obtain the effective kernel matrix via Equation 7. The left top panel in Figure 3 displays the heatmap for the corresponding pathology kernel in Equation 12 evaluated at the grid of 30 points between  $[0, 1]$ . The left bottom panel in Figure 3 shows the sample functions generated from the effective GP as a prior using the pathology kernel learned from the plentiful data. Here, we remark that sampling function from DGP prior models is non-trivial as we did not find many instances in the literature except (Duvenaud et al., 2014; Dunlop et al., 2018). In the end, the regression with the rare data  $\{\mathbf{X}_r, \mathbf{y}_r\}$  can be done with optimizing the evidence of  $\mathbf{y}_r$ . In the present experiment, we set the  $\ell = 1$  in the pathology kernel and employ grid search for the optimal values for  $\sigma_2$  and  $\ell_2$ . The panel (a) in Figure 4 shows the regression result where the predictive uncertainty substantially improves upon the result from directly applying GP with the rare data, which can be found in the Supplemental Material (Fig.6 right panel). In particular, one may note that there is no data for  $y_r$  in the region  $x < 0.4$  but our prediction mean is still close to the truth and the uncertainty is small. The result from direct application of standard GP sees similar predictive mean but the uncertainty is very large for  $x < 0.2$ .

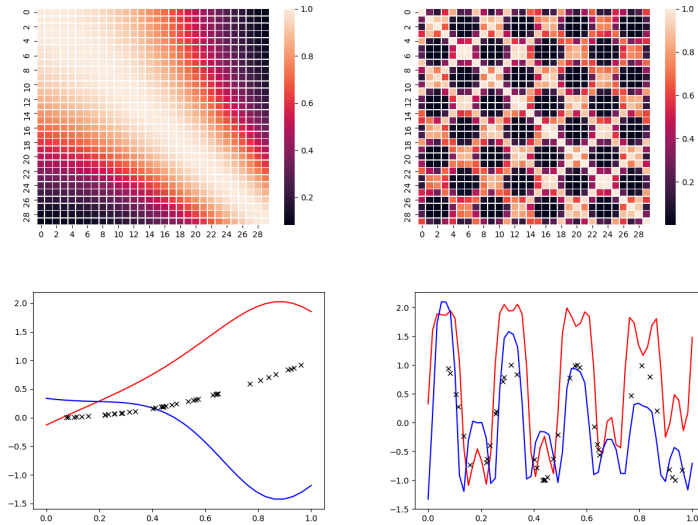


Figure 3: Heatmap illustration of the data-driven kernels learned from data generated by different functions. Bottom row shows random functions sampled from the effective kernel. The input is grid of size 30 points in the interval  $[0,1]$ . The hyperparameters  $\sigma_2 = 1$  and  $\ell_2 = 0.5$ . Left top: the data kernel learned from the plentiful data from  $y = x^2$ . Brighter (darker) colors represent stronger (weaker) covariance. Left bottom: Two sampled functions shown in blue and red colors while the black cross symbols represent the plentiful data. Right top: periodicity shown in the learned kernel with data from  $y = \sin 8\pi x$ . Right bottom: two sampled functions display multi-length scales which originate from data as well as the deep model.

For comparison with the simulation results in (Cutajar et al., 2019), we follow the nonlinear-A example there and generate 30 plentiful data from the function  $y = g(x) = \sin 8\pi x$  and 10 rare data from  $y = (x - \sqrt{2})g^2(x)$ . Learning from the plentiful data leads to the effective pathology kernel in the right top panel in Figure 3. Apparently, the learned covariance has a very different structure than that learned from the previous case, which shows the flexibility of our kernel learning. Two random functions are sampled from the corresponding GP and are displayed in the right bottom panel. It can be seen that the sampled functions possess the length scale learned from the low-fidelity function, and additional length scales which may originate from the deep model can be found too. Finally, we use the rare data for our effective GP regression, and the prediction is shown in the panel (b) of Figure 4. In the present simulation, there are 30 random data as  $\mathbf{y}_p$  and 10 as  $\mathbf{y}_r$ , and the corresponding result using the code of Cutajar et al. (2019) can be found in panel (c) of Figure 4. The two methods show similar accuracy and tight uncertainty near the region where the rare data is available. In the region where no rare data is seen, on the other hand, our method demonstrates more accurate prediction (black curve) and tighter uncertain region between the blue dashed curves.

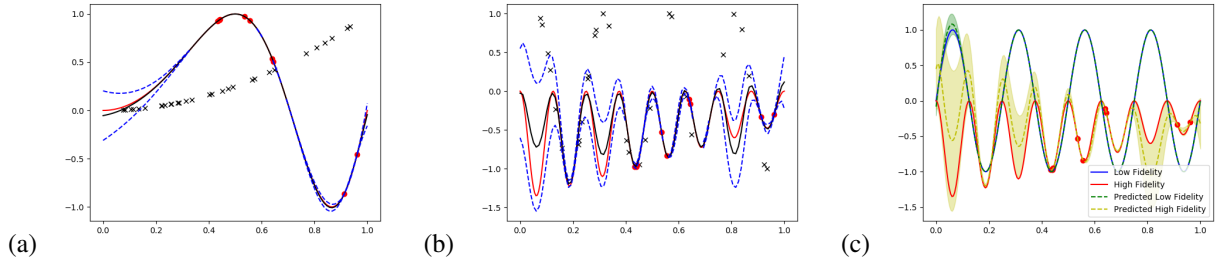


Figure 4: Regressions with two sources of data of high (red circle symbol) and low (cross symbol) fidelity. The high-fidelity data is generated from the precise observation of the truth function (red curve). The predictive mean is illustrated with black solid curve, regions between the blue dashed curves are predictive uncertainty. (a) The rare data from  $y = \sin 2\pi x^2$  and the plentiful data from  $y = x^2$ . (b) plentiful data from  $y = g(x) = \sin 8\pi x$  and rare data from  $y = (x - \sqrt{2})g^2(x)$ . (c) The same data as in panel b and comparing with MF-DGP package for regression.

## 6.2 Noisy&noise-free data

Unlike the above cases where the plentiful data has a fixed relation with the rare data, the noise-free data can not be obtained by sending the noisy data through some predetermined transformation. Nevertheless, if we regard the marginalization over  $h$  in Equation 13 as a kind of *model averaging* Goodfellow et al. (2016), we shall expect tighter variance from the present regression algorithm.

In figure 5, we demonstrate the regression result with 40 noisy and random data in  $\{\mathbf{X}_p, \mathbf{y}_p\}$  from the high-fidelity function in the nonlinear-A example, i.e,  $y = (x - \sqrt{2})g^2(x) + 0.25\epsilon$  with  $\epsilon \sim \mathcal{N}(0, 1)$ , and 10 noise-free data from the same function. The black cross symbols represent the noisy data while the red circles for the noise-free ones. The light-blue curve and the shadow region represent the predictive mean and uncertainty from applying RBF-GP to the union of both data. The relatively large noise and the lack of data in some regions result in significant uncertainty around the prediction. The predictive mean and uncertainty are presented by the black curve and blue dashed curves, respectively. The predictions from both methods are similar, but the uncertainty in our method is much tighter, which is expected from the model averaging perspective.

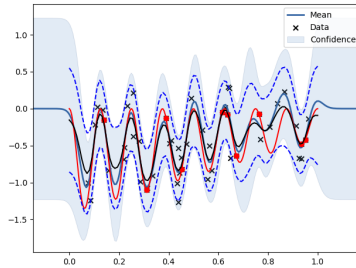


Figure 5: Regression with 40 noisy (cross symbol) and 10 precise (red circle) data generated by the ground truth function (red curve using the function  $y = (x - \sqrt{2})g^2(x)$  in previous example). GP is directly applied to the union of both noisy and precise observations, and the resultant predictive mean and variance are illustrated by the navy blue line and shadow regions. Our multi-source DGP kernel learning algorithm, on the other hand, connects the noisy data with the first layer GP and the precise data with the second GP. The resultant prediction, made by GP with effective kernel, is characterized by the mean (black curve) and covariance (between blue dashed curves).

## 7 Conclusion

In this paper we propose a novel kernel learning inspired from the multi-source Deep Gaussian Process structure. Our approach addresses two limitations of prior research on GPs: the need to choose a kernel and the lack of explicit dependence on the observations in the predictive covariance. We resolve limitations associated with reliance on experts to choose kernels, introducing new data-dependent kernels together with effective approximate inference. Our results show that the method is effective, and we prove that our moment-matching approximation retains some of multi-scale

and long-ranged correlation that are characteristic of deep models. We resolve limitations associated with lack of explicit dependence on observations in the predictive covariance by introducing the data-driven kernel. Our results show the benefits of joint dependence on the input and the predicted variables in reduced uncertainty in regions with sparse observations (e.g. Figure 4).

Central to the allure of Bayesian methods, including Gaussian Processes, is the ability to calibrate model uncertainty through marginalization over hidden variables. The power and promise of deep GP is in allowing rich composition of functions while maintaining the Bayesian character of inference over unobserved functions. Whereas most approaches are based on variational approximations for inference and Monte Carlo sampling in prediction stage, our approach uses a moment-based approximation in which deep GP is an analytically approximated with a GP. For both, the full implications of these approximations are unknown. Through analysis of higher moments, we can show that our approach retains some of important signatures of deep models, while avoiding the need for further optimization or sample-based approximation. Continued research is required to understand the full strengths and limitations of each approach.

## Appendix

From the true DGP distribution given in the main text, it can be shown with the theorem in Isserlis (1918) that the fourth moment is the sum,

$$\mathbb{E}[f_i f_j f_m f_l] = \mathbb{E}_{p(h)}[k_2(h_i, h_j)k_2(h_l, h_m)] + \mathbb{E}_{p(h)}[k_2(h_i, h_l)k_2(h_j, h_m)] + \mathbb{E}_{p(h)}[k_2(h_i, h_m)k_2(h_j, h_l)], \quad (15)$$

where the distribution for the quartet  $h_{i,j,m,l}$  is a multivariate Gaussian distribution,  $p(h_{i,j,m,l}) = \mathcal{N}(\mathbb{V}_4, \mathbb{K}_4)$  specified by its mean vector  $\mathbb{V}_4$  and covariance matrix  $\mathbb{K}_4$ ,

$$\mathbb{V}_4 = \begin{bmatrix} \mu_i \\ \mu_j \\ \mu_m \\ \mu_l \end{bmatrix},$$

and

$$\mathbb{K}_4 = \begin{bmatrix} k_{ii} & k_{ij} & k_{im} & k_{il} \\ k_{ij} & k_{jj} & k_{jm} & k_{jl} \\ k_{im} & k_{jm} & k_{mm} & k_{ml} \\ k_{il} & k_{jl} & k_{ml} & k_{ll} \end{bmatrix}.$$

We shall focus on the first term in the sum,

$$k_2(h_i, h_j)k_2(h_m, h_l) = \cos^2 \frac{h_i - h_j}{2} \cos^2 \frac{h_m - h_l}{2},$$

which can be expressed as the exponential form,

$$\frac{1}{4} + \frac{1}{8}[e^{i(h_i - h_j)} + \dots] + \frac{1}{16}[e^{i(h_i - h_j + h_m - h_l)} + \dots], \quad (16)$$

where there are a total of 4 similar terms involving  $h_{m,l}$  in the first bracket. In the second bracket, there are also 4 similar terms with different sign combinations. Next we can apply the identity  $\mathbb{E}_{p(\mathbf{h})}[e^{\mathbf{u} \cdot \mathbf{h}}] = \exp(\mathbf{u} \cdot \mathbb{V} + \frac{\mathbf{u}^T \mathbb{K} \mathbf{u}}{2})$  valid for both two-dimension and four-dimension cases. One can show that

$$\mathbb{E}_{p(h)}[e^{i(h_i - h_j)}] = e^{i(\mu_i - \mu_j)} \exp\left(\frac{2k_{ij} - k_{ii} - k_{jj}}{2}\right), \quad (17)$$

and

$$\mathbb{E}_{p(h)}[e^{i(h_i - h_j + h_m - h_l)}] = e^{i(\mu_i - \mu_j + \mu_m - \mu_l)} \exp\left(\frac{2k_{ij} - k_{ii} - k_{jj}}{2}\right) \exp\left(\frac{2k_{ml} - k_{mm} - k_{ll}}{2}\right) \exp(V_{ij,ml}) \quad (18)$$

where we denote the exponential cross term  $V_{ij,ml} = k_{il} + k_{jm} - k_{im} - k_{jl}$ , and the plus/minus is associated with the sign in the exponent of  $\exp[\pm i(h_i - h_j + h_m - h_l)]$  in  $\mathbb{E}[\cdot]$ . Now we can first collect the terms and obtain the second moment,

$$\mathbb{E}[f_i f_j] = \frac{1 + \cos(\mu_i - \mu_j)e^{V_{ij}}}{2}, \quad (19)$$

where the two-indices symbol  $V_{ij} = 2k_{ij} - k_{ii} - k_{jj}$ . Similarly, the fourth moment is given by,

$$\begin{aligned} \mathbb{E}_{p(h)}[k_2(h_i, h_j)k_2(h_l, h_m)] &= \frac{1 + \cos(\mu_i - \mu_j)e^{V_{ij}} + \cos(\mu_m - \mu_l)e^{V_{ml}}}{4} + \\ &e^{V_{ij} + V_{ml}} \left[ \frac{\cos(\mu_i - \mu_j + \mu_m - \mu_l)}{8} e^{V_{ij,ml}} + \frac{\cos(\mu_i - \mu_j - \mu_m + \mu_l)}{8} e^{-V_{ij,ml}} \right]. \quad (20) \end{aligned}$$

Comparing with the expression for the second moment, the difference  $\mathbb{E}_{p(h)}[k_2(h_i, h_j)k_2(h_l, h_m)] - \mathbb{E}[f_i f_j] \mathbb{E}[f_m f_l]$  now reads,

$$e^{V_{ij}+V_{ml}} \left[ \frac{\cos(\mu_i - \mu_j + \mu_m - \mu_l)}{8} e^{V_{ij,ml}} + \frac{\cos(\mu_i - \mu_j - \mu_m + \mu_l)}{8} e^{-V_{ij,ml}} - \frac{\cos(\mu_i - \mu_j) \cos(\mu_m - \mu_l)}{4} \right].$$

Note that  $V_{ij} < 0$  and  $V_{ij,ml}$  can be positive or negative. The remaining two terms in the sum Eq. (1) follow identical derivation, thus we complete the proof of Lemma 4.

## Supplemental Material

Here we present the comparison with the results obtained by directly applying RBF-GP (GPpy package) GPpy (2012). We generate randomly 30 points as  $\mathbf{X}_p$  and 10 points as  $\mathbf{X}_r$  using `np.random.rand` function in numpy with random seed of 59. The data  $\{\mathbf{X}_p, \mathbf{y}_p\}$  (black cross) serves as relevant information to the target knowledge (red line) which is partially known through the rare data  $\{\mathbf{X}_r, \mathbf{y}_r\}$  (red circle). The predictive mean and variance are displayed with black solid line and blue dashed lines, respectively. We also use the examples from the nonlinear-A (Fig. 7) and nonlinear-B (Fig. 8) cases in Cutajar et al. (2019).

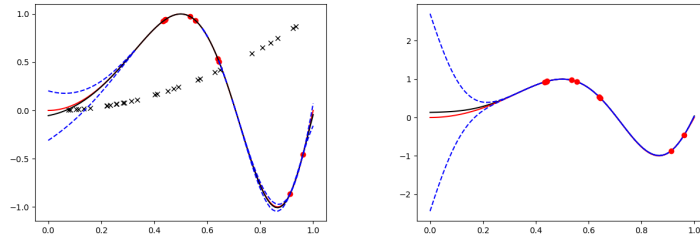


Figure 6: Regression with rare data (red circle) generated from  $y = \sin 2\pi x^2$ . Left panel: first learn kernel from the plentiful data (black cross) generated from  $y = x^2$  and subsequently apply effective GP. Right panel: directly applying RBF-GP with the rare data. The uncertainty in left panel is significantly reduced in comparison with the right panel.

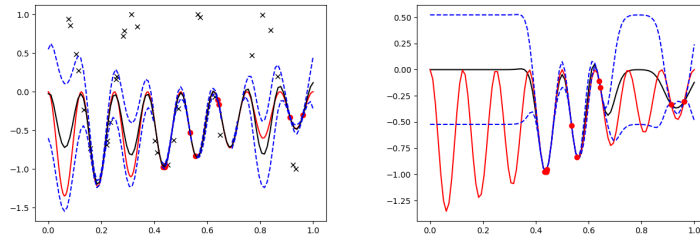


Figure 7: Nonlinear A case in Cutajar et al. (2019). Plentiful data generated from  $y = g(x) = \sin 8\pi x$  and the rare data from  $y = (x - \sqrt{2})g^2(x)$ . Left: kernel learning from plentiful data followed by effective GP inference. Right: directly applying RBF-GP with the rare data.

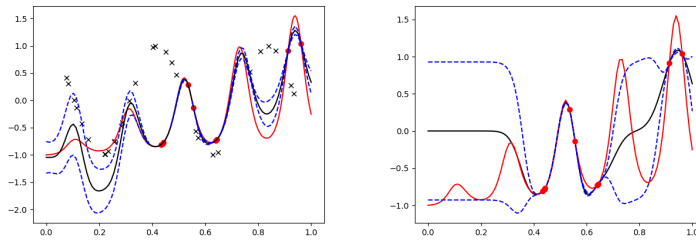


Figure 8: Nonlinear B case in Cutajar et al. (2019). We use  $y = g(x) = \cos 15x$  to generate the plentiful data for kernel learning with the goal to perform the regression task for the rare data generated from  $y = \exp[g(2x - 0.2)] - 1$ . Left panel: our method. Right panel: directly apply RBF-GP with the rare data.

## References

- Agrawal, D., Papamarkou, T., and Hinkle, J. (2020). Wide neural networks with bottlenecks are deep gaussian processes. *arXiv preprint arXiv:2001.00921*.
- Alain, G. and Bengio, Y. (2014). What regularized auto-encoders learn from the data-generating distribution. *The Journal of Machine Learning Research*, 15(1):3563–3593.
- Álvarez, M. A. and Lawrence, N. D. (2011). Computationally efficient convolved multiple output gaussian processes. *Journal of Machine Learning Research*, 12(May):1459–1500.
- Bengio, Y., Yao, L., Alain, G., and Vincent, P. (2013). Generalized denoising auto-encoders as generative models. In *Advances in neural information processing systems*, pages 899–907.
- Cho, Y. and Saul, L. K. (2009). Kernel methods for deep learning. In *Advances in neural information processing systems*, pages 342–350.
- Cutajar, K., Pullin, M., Damianou, A., Lawrence, N., and González, J. (2019). Deep gaussian processes for multi-fidelity modeling. *arXiv preprint arXiv:1903.07320*.
- Damianou, A. and Lawrence, N. (2013). Deep gaussian processes. In *Artificial Intelligence and Statistics*, pages 207–215.
- Daniely, A., Frostig, R., and Singer, Y. (2016). Toward deeper understanding of neural networks: The power of initialization and a dual view on expressivity. In *NIPS*.
- Dunlop, M. M., Girolami, M. A., Stuart, A. M., and Teckentrup, A. L. (2018). How deep are deep gaussian processes? *The Journal of Machine Learning Research*, 19(1):2100–2145.
- Duvenaud, D., Lloyd, J. R., Grosse, R., Tenenbaum, J. B., and Ghahramani, Z. (2013). Structure discovery in nonparametric regression through compositional kernel search. *arXiv preprint arXiv:1302.4922*.
- Duvenaud, D., Rippel, O., Adams, R., and Ghahramani, Z. (2014). Avoiding pathologies in very deep networks. In *Artificial Intelligence and Statistics*, pages 202–210.
- Goodfellow, I., Bengio, Y., and Courville, A. (2016). *Deep learning*. MIT press.
- GPy (since 2012). GPy: A gaussian process framework in python. <http://github.com/SheffieldML/GPy>.
- Havasi, M., Hernández-Lobato, J. M., and Murillo-Fuentes, J. J. (2018). Inference in deep gaussian processes using stochastic gradient hamiltonian monte carlo. In *Advances in Neural Information Processing Systems*, pages 7506–7516.
- Hensman, J., Fusi, N., and Lawrence, N. D. (2013). Gaussian processes for big data. In *Uncertainty in Artificial Intelligence*, page 282. Citeseer.
- Hinton, G. E. and Salakhutdinov, R. R. (2008). Using deep belief nets to learn covariance kernels for gaussian processes. In *Advances in neural information processing systems*, pages 1249–1256.
- Isserlis, L. (1918). On a formula for the product-moment coefficient of any order of a normal frequency distribution in any number of variables. *Biometrika*, 12(1/2):134–139.
- Jacot, A., Gabriel, F., and Hongler, C. (2018). Neural tangent kernel: Convergence and generalization in neural networks. In *Advances in neural information processing systems*, pages 8571–8580.

- Janati, H., Cuturi, M., and Gramfort, A. (2019). Wasserstein regularization for sparse multi-task regression. In *The 22nd International Conference on Artificial Intelligence and Statistics*, pages 1407–1416.
- Kaiser, M., Otte, C., Runkler, T., and Ek, C. H. (2018). Bayesian alignments of warped multi-output gaussian processes. In *Advances in Neural Information Processing Systems*, pages 6995–7004.
- Karakida, R., Akaho, S., and Amari, S.-i. (2019). Universal statistics of fisher information in deep neural networks: Mean field approach. In *The 22nd International Conference on Artificial Intelligence and Statistics*, pages 1032–1041.
- Kazlauskaitė, I., Ek, C. H., and Campbell, N. (2019). Gaussian process latent variable alignment learning. In *The 22nd International Conference on Artificial Intelligence and Statistics*, pages 748–757.
- Kennedy, M. C. and O’Hagan, A. (2000). Predicting the output from a complex computer code when fast approximations are available. *Biometrika*, 87(1):1–13.
- Lázaro-Gredilla, M. (2012). Bayesian warped gaussian processes. In *Advances in Neural Information Processing Systems*, pages 1619–1627.
- Lee, J., Bahri, Y., Novak, R., Schoenholz, S. S., Pennington, J., and Sohl-Dickstein, J. (2017). Deep neural networks as gaussian processes. *arXiv preprint arXiv:1711.00165*.
- Lu, C.-K., Yang, S. C.-H., Hao, X., and Shafto, P. (2019). Interpretable deep gaussian processes with moments. *arXiv preprint arXiv:1905.10963*.
- Moreno-Muñoz, P., Artés-Rodríguez, A., and Álvarez, M. A. (2018). Heterogeneous multi-output Gaussian process prediction. In *Advances in Neural Information Processing Systems (NeurIPS) 31*.
- Neal, R. M. (2012). *Bayesian learning for neural networks*, volume 118. Springer Science & Business Media.
- Perdikaris, P., Raissi, M., Damianou, A., Lawrence, N., and Karniadakis, G. E. (2017). Nonlinear information fusion algorithms for data-efficient multi-fidelity modelling. *Proceedings of the Royal Society A: Mathematical, Physical and Engineering Sciences*, 473(2198):20160751.
- Poole, B., Lahiri, S., Raghu, M., Sohl-Dickstein, J., and Ganguli, S. (2016). Exponential expressivity in deep neural networks through transient chaos. In *NIPS*.
- Raissi, M. and Karniadakis, G. (2016). Deep multi-fidelity gaussian processes. *arXiv preprint arXiv:1604.07484*.
- Rasmussen, C. E. and Williams, C. K. I. (2006). *Gaussian Process for Machine Learning*. MIT press, Cambridge, MA.
- Salimbeni, H. and Deisenroth, M. (2017). Doubly stochastic variational inference for deep gaussian processes. In *Advances in Neural Information Processing Systems*.
- Shah, A., Wilson, A., and Ghahramani, Z. (2014). Student-t processes as alternatives to gaussian processes. In *Artificial intelligence and statistics*, pages 877–885.
- Snelson, E. and Ghahramani, Z. (2006). Sparse gaussian processes using pseudo-inputs. In *Advances in neural information processing systems*, pages 1257–1264.
- Snelson, E., Ghahramani, Z., and Rasmussen, C. E. (2004). Warped gaussian processes. In *Advances in neural information processing systems*, pages 337–344.
- Steinke, F. and Schölkopf, B. (2008). Kernels, regularization and differential equations. *Pattern Recognition*, 41(11):3271–3286.
- Titsias, M. (2009). Variational learning of inducing variables in sparse gaussian processes. In *Artificial Intelligence and Statistics*, pages 567–574.
- Titsias, M. and Lawrence, N. (2010). Bayesian gaussian process latent variable model. In *Proceedings of the Thirteenth International Conference on Artificial Intelligence and Statistics*, pages 844–851.
- Williams, C. K. (1997). Computing with infinite networks. In *Advances in neural information processing systems*, pages 295–301.
- Wilson, A. G., Hu, Z., Salakhutdinov, R., and Xing, E. P. (2016). Deep kernel learning. In *Artificial Intelligence and Statistics*, pages 370–378.
- Yang, G. (2019). Scaling limits of wide neural networks with weight sharing: Gaussian process behavior, gradient independence, and neural tangent kernel derivation. *arXiv preprint arXiv:1902.04760*.